Heterogeneous dynamics in polycrystal and glass in a binary mixture with changing size dispersity and composition

Toshiyuki Hamanaka and Akira Onuki
Department of Physics, Kyoto University, Kyoto 606-8502, Japan
(Received 26 December 2006; published 25 April 2007)

Using molecular dynamics simulation we investigate the dynamics in a two-dimensional binary mixture at a low temperature and at high densities. We increase the size ratio of the diameters of the two components or the fraction of the larger particles. Then changeovers occur from polycrystal to glass with proliferation of defects. The relationship between the degree of disorder and the slow dynamics is studied by simultaneous visualization of a disorder variable D_j introduced in our previous paper T. Hamanaka and A. Onuki[Phys. Rev. E **74**, 011506 (2006)] and the particle displacement $\Delta \boldsymbol{r}_j$ in a long time interval. In polycrystal, the particles in the grain boundary regions have large D_j and a relatively large mobility, producing significant dynamic heterogeneity on long time scales. In the crossover from polycrystal to glass, the crystalline regions become narrow, but the particles with relatively large D_j still trigger the formation of chainlike particle motions, leading to the dynamic heterogeneity.

DOI: 10.1103/PhysRevE.75.041503 PACS number(s): 61.43.−j, 61.72.−y, 64.70.Pf

I. INTRODUCTION

A large number of molecular dynamics simulations have been performed to study the liquid-glass transition in two-dimensional (2D) and three-dimensional (3D) binary mixtures [1–10], where the time scale of the particle motions becomes dramatically slowed down with lowering of the temperature T. The size ratio σ_2/σ_1 of the diameters σ_1 and σ_2 of the two components has been chosen to maximize disruption of the crystal structure. As a salient feature, significant heterogeneity in the cooperative particle motions on long time scales has been reported, where successive stringlike motions form large-scale clusters growing at low temperatures. In particular, the heterogeneity correlation length ξ was determined from the distribution of broken bonds in 2D and 3D [3] and by a four-point dynamic susceptibility in 3D [8]. Recently attention has been paid to the connection between the structure and the slow dynamics. Vollmayr-Lee *et al.* [11] found in 3D that mobile particles (in their definition) are surrounded by fewer neighbors than the others. Widmer-Cooper and Harrowell [12] detected a clear correlation between the short-time heterogeneity in a local Debye-Waller factor and the long-time dynamic heterogeneity in 2D. In their one-component model with fivefold pair interaction in 2D, Shintani and Tanaka [13] introduced medium-range crystalline order strongly correlated to the slow dynamics in glass.

Also varying the size ratio σ_2/σ_1 as well as T [14–16], we have recently investigated changeovers among crystal, polycrystal, and glass at fixed composition in 2D [17]. For weak size dispersity and at low T, the mixture is in a crystal state with a small number of defects. With increasing σ_2/σ_1, polycrystal and glass states are subsequently realized. These three states can be distinguished using a disorder variable D_j supported by each particle j, since snapshots of D_j are highly heterogeneous in polycrystal and glass. The grain boundaries are pinned in the presence of size dispersity, while they emerge as rapidly varying thermal fluctuations near the 2D melting in one-component systems.

In this paper, we aim to investigate the dynamics in polycrystal and glass in a model binary mixture with size dispersity using the disorder variable D_j, the particle displacement $\Delta \boldsymbol{r}_j$, and the bond breakage [3]. We may then study the relationship between the local disorder at a particular time and the dynamic heterogeneity obtained from the particle configurations at two times much separated. The origin of the dynamic heterogeneity will turn out to be rather obvious for polycrystal. We thus study the crossover from polycrystal to glass, where local crystalline order is appreciable.

The organization of this paper is as follows. In Sec. II A, we will explain our method and introduce the disorder variable D_j. We will then visualize D_j and $\Delta \boldsymbol{r}_j$ in Sec. II B and calculate the time correlation function and the mean square displacement in Sec. II C. In Sec. II D, we will examine the distribution of the displacements and that of the broken bonds as a function of a parameter S representing the degree of disorder.

II. NUMERICAL RESULTS

A. Method and disorder variable

As in our previous paper [17], we performed molecular dynamics simulation of a 2D binary mixture interacting via a truncated Lenard-Jones potential of the form $v_{\alpha\beta}(r) = 4\epsilon[(\sigma_{\alpha\beta}/r)^{12} - (\sigma_{\alpha\beta}/r)^6] - C_{\alpha\beta}$ $(\alpha, \beta = 1, 2)$, characterized by the energy ϵ and the soft-core diameter $\sigma_{\alpha\beta} = (\sigma_\alpha + \sigma_\beta)/2$. For $r > r_{\rm cut} = 3.2\sigma_1$, we set $v_{\alpha\beta}(r) = 0$ and the constant $C_{\alpha\beta}$ ensures the continuity of $v_{\alpha\beta}(r)$ at the cutoff $r = r_{\rm cut}$. The total particle number is fixed at $N = N_1 + N_2 = 1000$. The volume V is chosen such that the volume fraction of the soft-core regions is fixed at 0.9 or

$$\phi = (N_1\sigma_1^2 + N_2\sigma_2^2)/V = 0.9. \tag{2.1}$$

With the mass ratio being $m_1/m_2 = (\sigma_1/\sigma_2)^2$, we integrated the Newton equations using the leapfrog algorithm under the periodic boundary condition. The temperature was controlled

with the Nose-Hoover thermostat [18]. The time step of integration is 0.002τ with

$$\tau = \sigma_1 \sqrt{m_1/\epsilon}. \tag{2.2}$$

Hereafter we will measure time in units of τ. We first equilibrated the system in a liquid state at $T=2\epsilon/k_B$ in a time interval of 10^3 and then quenched it to the final temperature $T=0.2\epsilon/k_B$. The total simulation time was 2.2×10^4 for each run. After a relaxation time of order 5000, there was no appreciable time evolution in various quantities obtained as an average over the particles (see Fig. 7 of Ref. [17]). There was also no tendency of phase separation in all the simulations in our previous and present papers (see Fig. 1 of Ref. [17], as an example). However, our simulation time became comparable to the structural relaxation time τ_α in glass at the largest $\sigma_2/\sigma_1=1.4$. Much longer simulation times are thus needed for a more quantitative analysis of such slow structural relaxations.

We consider a deviation from the hexagonal order for each particle j. In this work, the two particles $j\in\alpha$ and $k\in\beta$ are bonded if their distance $|\boldsymbol{r}_j-\boldsymbol{r}_k|$ is shorter than $1.5\sigma_{\alpha\beta}$ [3]. For each j, we consider the sum [19]

$$\chi_j = \sum_{k\in\text{bonded}} \exp[6i\theta_{jk}]$$

$$= |\chi_j| e^{6i\alpha_j}, \tag{2.3}$$

where θ_{jk} is the angle of the relative vector $\boldsymbol{r}_k-\boldsymbol{r}_j$ with respect to the x axis. The angle α_j defined in the second line represents the sixfold orientation order. The correlation function $g_6(r)$ of the space-dependent quantity $\Sigma_j\chi_j\delta(\boldsymbol{r}_j-\boldsymbol{r})$ has been calculated for one-component systems [20]. See item (viii) in the last section for results on $g_6(r)$ in our system. In our previous work [17], we constructed another nonnegative-definite variable representing the degree of disorder for each particle j by

$$D_j = 2\sum_{k\in\text{bonded}} [1-\cos 6(\alpha_j-\alpha_k)]. \tag{2.4}$$

For a perfect crystal at low T this quantity arises from the thermal vibrations and is nearly zero, but for particles around defects it assumes large values in the range 5–20. The average $\bar{D}=\Sigma_j D_j/N$ over the particles conveniently represents the degree of overall disorder, which is small in crystal and large in glass and liquid. To distinguish between glass and liquid, we furthermore need to examine the dynamics.

We performed two series of simulations. In one series we increase the size ratio σ_2/σ_1 at $N_1=N_2=500$. In the other series we increase the fraction of large particles,

$$c = N_2/N, \tag{2.5}$$

at $\sigma_2/\sigma_1=1.4$. In Fig. 1, the curve of $\bar{D}$ vs σ_2/σ_1 at $c=0.5$ and that of $\bar{D}$ vs c at $\sigma_2/\sigma_1=1.4$ are presented [21]. They are taken in steady states at $T=0.2\epsilon/k_B$ and $\phi=0.9$. The former curve was already presented in Fig. 8 in our previous paper [17].

As can be seen in Fig. 2, crystal, polycrystal, and glass are realized with increasing σ_2/σ_1 or c. On the curve for the first series, crystal states with only a few defects are realized for $\sigma_2/\sigma_1\lesssim1.15$, but defects are abruptly proliferated for $\sigma_2/\sigma_1\gtrsim1.2$. On that for the second series, defects are always generated around each large particle (see the right panel of Fig. 3 below) leading to a strong increase $\bar{D}\sim30c$ for $c\lesssim0.2$.

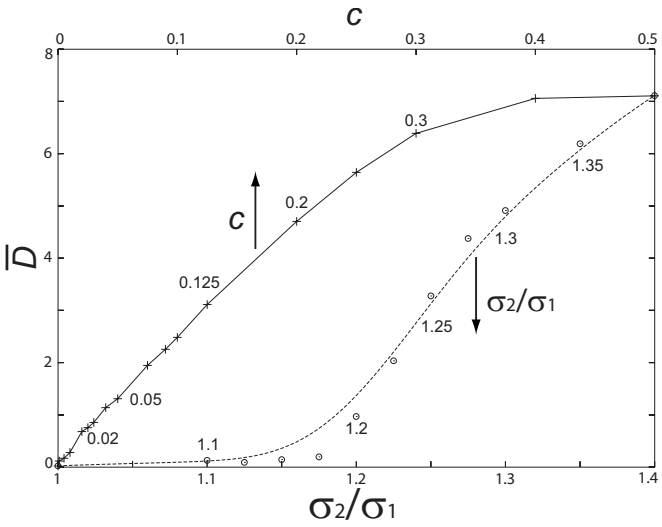

FIG. 1. Average disorder parameter $\bar{D}=\Sigma_j D_j/N$ at $T=0.2\epsilon/k_B$ and $\phi=0.9$ with changing the size ratio σ_2/σ_1 at $N_1=N_2=500$ (lower curve) [17] and with changing the fraction $c=N_2/N$ of the larger particles at $\sigma_2/\sigma_1=1.4$ (upper curve).

In our calculations (except those in Figs. 4–6), the particle positions used are the time averages taken over an interval with width 1. That is, the time average $\int_t^{t+1}dt'\boldsymbol{r}_j(t')$ was used in place of $\boldsymbol{r}_j(t)$. This short-time smoothing of the particle positions was also used in our previous paper [17].

B. Changeover with increasing size dispersity and composition

In Fig. 2, we show snapshots of D_j at $t=1.2\times10^4$ for (a) $\sigma_2/\sigma_1=1.2$, (b) 1.25, (c) 1.3, and (d) 1.35 in the first series and for (a′) $c=0.02$, (b′) 0.05, (c′)0.125, and (d′) 0.2 at $\sigma_2/\sigma_1=1.4$ in the second series. The color of the particles varies in the order of rainbow, being violet for $D_j=0$ and red for the maximum of D_j. The arrows are the displacement vectors from the particle position at this time to that at $t=2.2\times10^4$, where the width of the time interval is 10^4. Here the particles with displacement longer than σ_1 are called the mobile particles. In this visualization we clearly recognize polycrystal states intermediate between crystal and glass states. In the first series at $c=1/2$, defects are accumulated around the grain boundaries and the crystalline regions become narrow and ill defined rather abruptly around $\sigma_2/\sigma_1\sim1.25$. In the second series at $\sigma_2/\sigma_1=1.4$, the large particles form grain boundaries and the crystalline regions composed of the small particles are well ordered for small $c\lesssim0.125$. The crystalline regions are composed of the two components in the first series and of the smaller component only in the second series. We shall see a number of different dynamical effects in these two polycrystal states. In Fig. 3, the particle

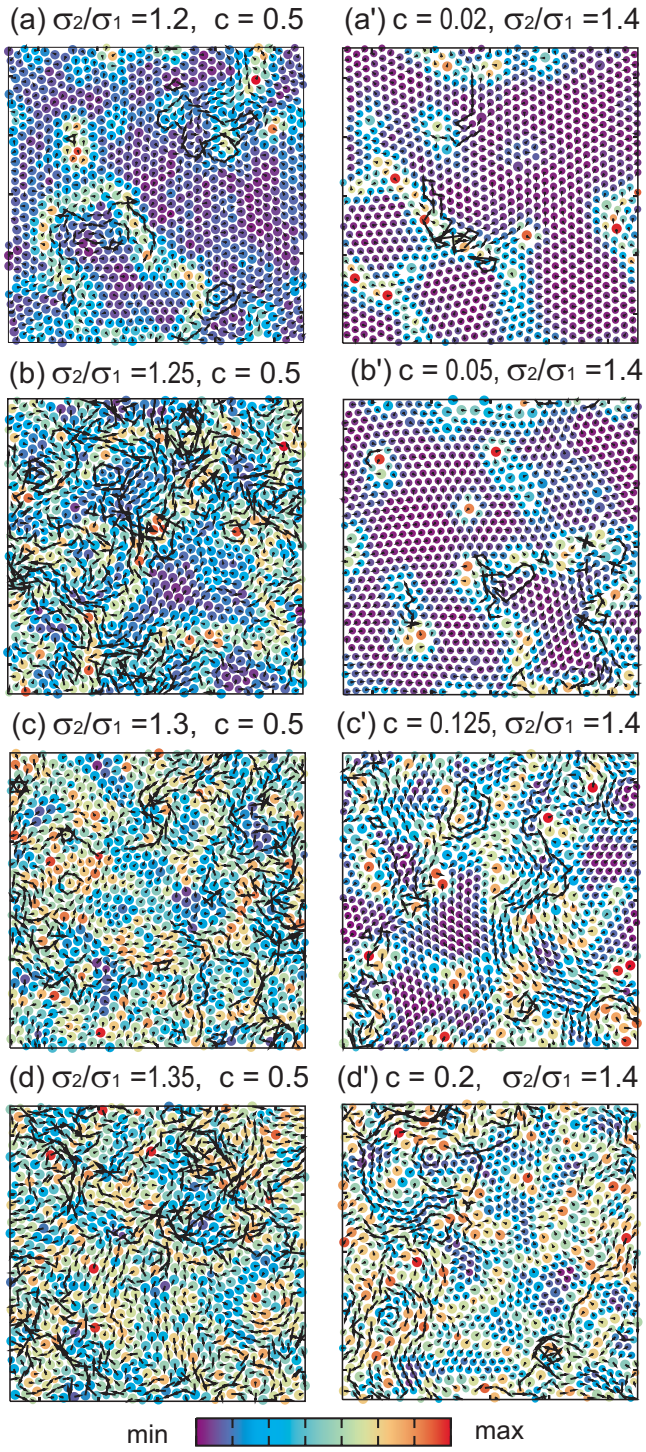

FIG. 2. (Color online) Disorder variable D_j in Eq. (2.4) at $T=0.2\epsilon/k_B$ and $\phi=0.9$. Left: (a) $\sigma_2/\sigma_1=1.2$, (b) 1.25, (c) 1.3, and (d) 1.35 at $c=0.5$. Right: (a′) $c=0.02$, (b′) 0.05, (c′)0.125, and (d)′ 0.2 at $\sigma_2/\sigma_1=1.4$. The arrows represent the particle displacement $\Delta \boldsymbol{r}_j$ in the subsequent time interval of width 10^4. The color is given to each picture independently, according to its minimum and maximum of D_j. The average of D_j in the crystalline regions is larger in (a) than in (a′)and (b′) (see Figs. 3 and 4), leading to the difference in color.

configurations around grain boundaries are shown for the polycrystal states (a) and (b′) in Fig. 2, where the circles have diameters σ_1 (in black) and σ_2 (in gray). We can hardly find the grain boundaries for (a) with Fig. 3 only, while the large particles are in the grain boundary regions for (b′).

We further discuss the dynamics revealed in Fig. 2. (i) At any σ_2/σ_1, mobile particles with large displacements form strings. With increasing σ_2/σ_1 in (a)–(d) and c in (a′)–(d′), such strings tend to aggregate, resulting in significant dynamic heterogeneities. This feature has been observed numerically in supercooled liquids and glass [3,4,7], but it can be seen here also in polycrystal with size dispersity. (ii) The mobile particles have relatively large D_j in many cases and, at least, particles with large D_j trigger the formation of the strings. Small particles bonded to a large particle frequently become mobile even when the large one remains immobile, which is evident in the second series (see the lower panel of Fig. 8 below also). (iii) In polycrystal states such as (a), (b), and (a′)–(d′) the mobile particles are mostly in the grain boundary regions with large D_j. The dynamic heterogeneity in polycrystal such as in (b) and (c′) is thus ascribed to a relatively high mobility of the particles in the grain boundary regions. (iv) In the glass states (c), (d), and (d′), the degree of disorder is enhanced and the grain boundaries become ill defined, but we can still see the aggregation of the strings extending longer than the heterogeneities of D_j. For $\sigma_2/\sigma_1=1.4$ and $c=1/2$ (see Fig. 4 of Ref. [17]), the mobile particles are considerably fewer than in (d), so a wider time interval is needed for visualization of the displacements. (v) In addition, in polycrystal and glass, crystalline regions consisting of small D_j can undergo collective motions induced by large displacements of the surrounding particles. Such motions will be clearly seen in expanded snapshots of Fig. 8. We recognize that they remain small in quiescent states, but we will show that they can be large in shear flow [see item (vii) in the last section].

We may consider the particle-number density as a function of the disorder variable D_j. Because the range $0<D_j \lesssim 20$ realized is rather wide, we use

$$S_j = \sqrt{D_j} \tag{2.6}$$

and define the number density

$$n(S) = \sum_{j=1}^{N} \langle \theta(S - S_j) \rangle / N, \tag{2.7}$$

where $\theta(x)$ is the step function, being 1 for $x>0$ and 0 for $x\leq 0$. The average $\langle \cdots \rangle$ in Eq. (2.7) is over the time and over five independent runs. In Fig. 4, we show the derivative $dn(S)/dS$, which is the distribution of the density as a function of S. The area below each curve is unity or $\int_0^\infty dS dn(S)/dS=1$. The peaks of the curves (a) and (a′) at small S arise from the particles forming crystalline regions. Notice that these peaks are separated by a small amount because the crystalline regions in (a′)are more frustrated (see Fig. 3). The distributions for the glass states (d) and (d′) are broad in the range $S\lesssim 4$, but a mild peak representing crystalline order still remains at $S\sim 0.5$ for (d′).

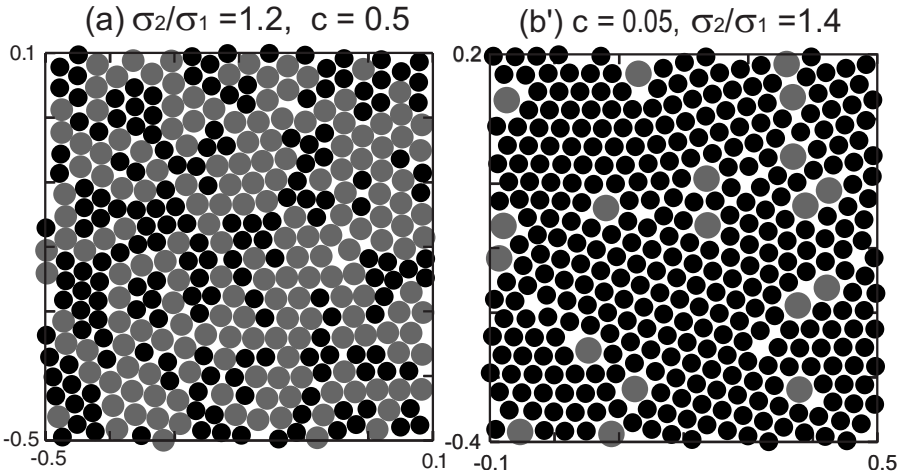

FIG. 3. Particles around grain boundaries, which are 36% of (a) and (b′) in Fig. 2. Left: the left and bottom parts of (a), where strings of the small particles are conspicuous. Right: the right and bottom parts of (b′), where the large particles form grain boundaries. The numbers at the corners are the coordinates. The total system is in the region $-0.5 \leq x \leq 0.5$ and $-0.5 \leq y \leq 0.5$ in the horizontal x and vertical y axes.

C. Time correlation function and mean-square displacement

We also examine the quantities constructed from the particle displacement,

$$\Delta \boldsymbol{r}_j(t) = \boldsymbol{r}_j(t+t_0) - \boldsymbol{r}_j(t_0), \tag{2.8}$$

of the small particles for various σ_2/σ_1 and c. Here we do not take the time average of the particle positions on a short time interval of width 1 to see the short-time ballistic motion (see the last sentence of Sec. II A). In Fig. 5, we display the self-time-correlation function

$$F_s(q,t) = \sum_{j=1}^{N_1} \langle \exp[i\boldsymbol{q} \cdot \Delta \boldsymbol{r}_j(t)] \rangle / N_1, \tag{2.9}$$

at $q = 2\pi/\sigma_1$. In Fig. 6, we show the mean square displacement

$$\langle [\Delta \boldsymbol{r}(t)]^2 \rangle = \sum_{j=1}^{N_1} \langle [\Delta \boldsymbol{r}_j(t)]^2 \rangle / N_1. \tag{2.10}$$

The average $\langle \cdots \rangle$ in Eqs. (2.9) and (2.10) [and in Eqs. (2.11) and (2.13) below] is taken over the initial time t_0 and over five independent runs.

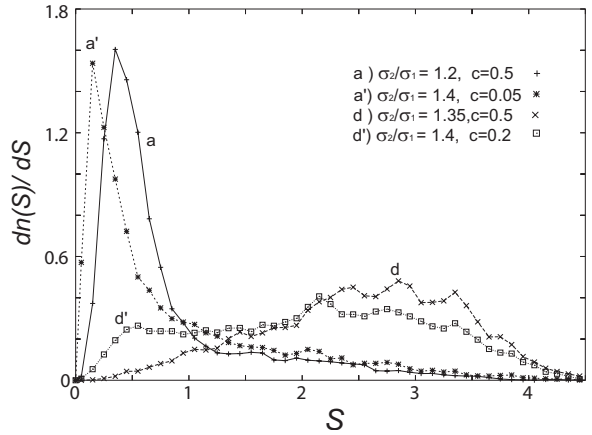

FIG. 4. Number-density distribution $dn(S)/dS$ as a function of the disorder variable S in Eq. (2.6) for the polycrystal states (a) and (a′) and for the glass states (d) and (d′).

In the first series, the long-time behaviors of these two quantities change abruptly from $\sigma_2/\sigma_1 = 1.2$ to 1.25, where D_j changes abruptly. In the second series, these two quantities change gradually with increasing c. We may determine the structural relaxation time τ_α by $F_s(q,\tau_\alpha) = e^{-1}$ at this

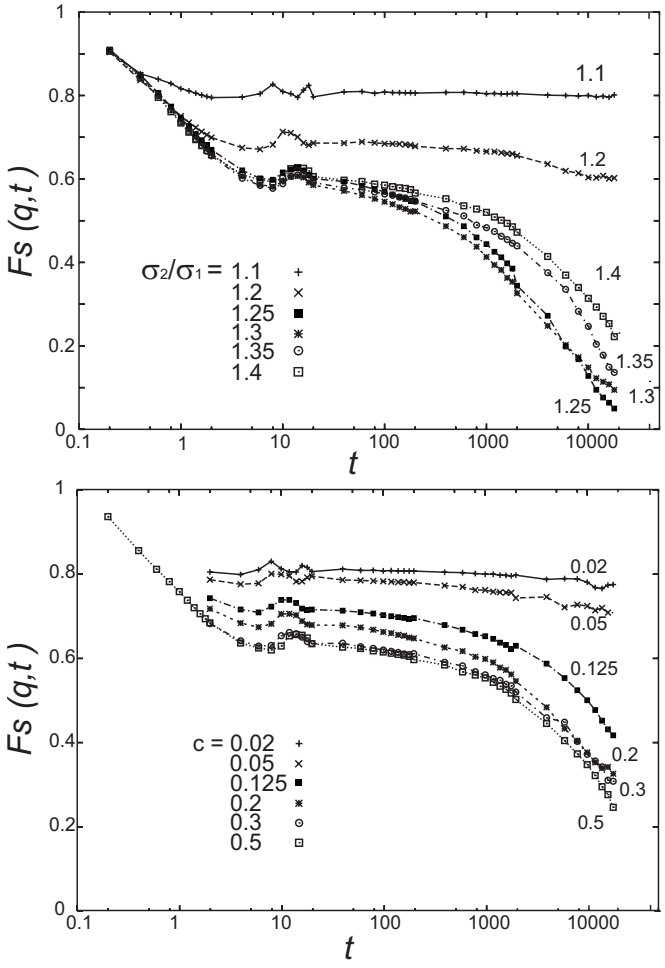

FIG. 5. Time correlation function $F_s(q,t)$ of the small particles at $q = 2\pi/\sigma_1$ in Eq. (2.9) for various σ_2/σ_1 (upper plate) and for various c (lower plate) on a semilogarithmic scale. The decay is fastest for $\sigma_2/\sigma_1 = 1.25$ in the upper plate, while it becomes faster with increasing c in the lower plate.

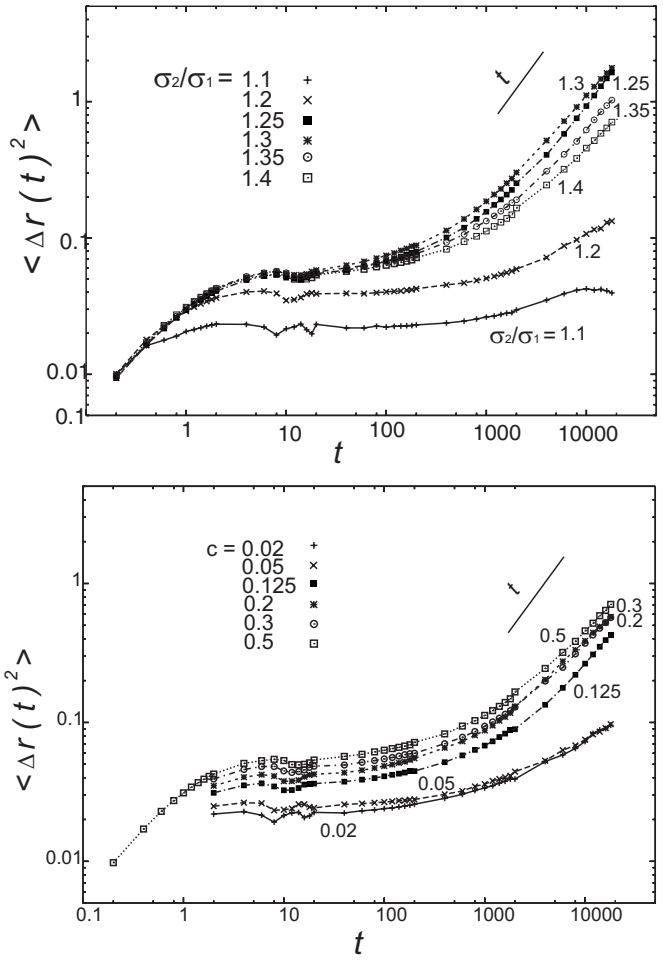

FIG. 6. Mean-square displacement $\langle[\Delta \boldsymbol{r}(t)]^2\rangle$ of the small particles in Eq. (2.10) for various σ_2/σ_1 (upper plate) and for various c (lower plate) on a logarithmic scale. It is nonmonotonic with increasing σ_2/σ_1 in the upper plate.

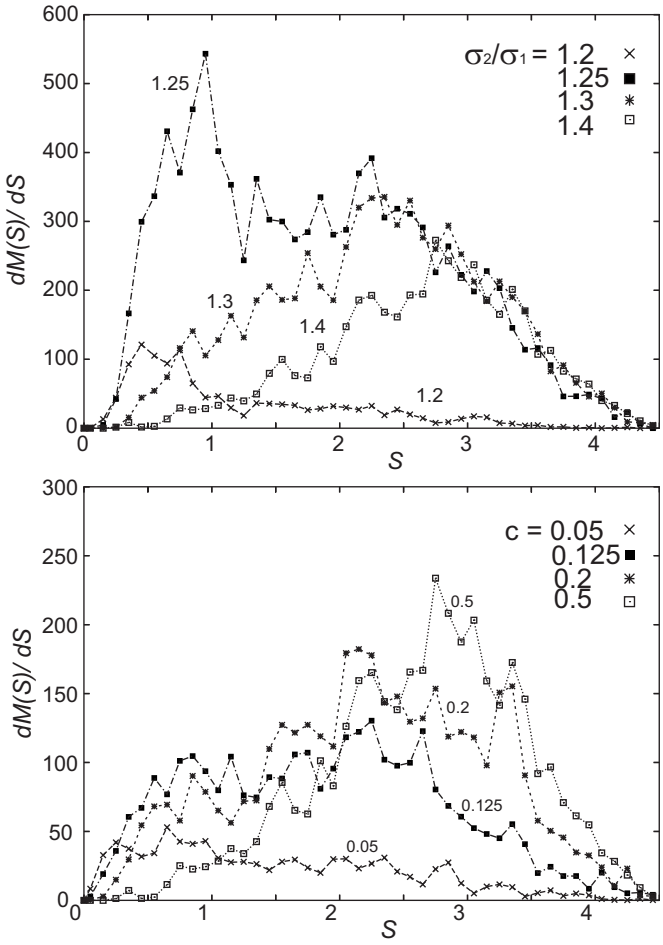

FIG. 7. Distribution of the mean-square displacement $dM(S)/dS$ as a function of the disorder variable S in Eq. (2.6) for various σ_2/σ_1 (upper plate) and for various c (lower plate). $M(s)$ is defined in Eq. (2.10). The curve of $\sigma_2/\sigma_1=1.25$ in the upper plate exhibits a large peak at small S exceptionally (see the text).

wave number [3]. In Fig. 6, we can see that the particle motions in short times ($\lesssim 1$) are ballistic or $\langle[\Delta \boldsymbol{r}(t)]^2\rangle \propto t^2$. The diffusive behavior $\langle[\Delta \boldsymbol{r}(t)]^2\rangle \cong 4Dt$ appears at large t for $\sigma_2/\sigma_1 \geq 1.3$ in the upper panel and for $c \geq 0.125$ in the lower panel in our simulation time, where D is the diffusion constant of a small tagged particle. For $\sigma_2/\sigma_1=1.25$, 1.3, 1.35, and 1.4 in the first series (upper panels), we have $\tau_\alpha=1.9$, 1.5, 4.3, and 6.1 in units of $10^3\tau$ and $D=2.3$, 2.7, 1.6, and 1.1 in units of $10^{-5}\sigma_1^2/\tau$, respectively. Remarkably, the relaxation of $F_s(q,t)$ is shortest and $\langle[\Delta \boldsymbol{r}(t)]^2\rangle$ is largest for a polycrystal state with $\sigma_2/\sigma_1 \cong 1.25$. For $c=0.125$, 0.2, and 0.4 in the second series (lower panels), we have $\tau_\alpha=2.2$, 1.1, and 0.64 in units of $10^4\tau$ and $D=0.66$, 0.97, and 1.3 in units of $10^{-5}\sigma_1^2/\tau$, respectively, where τ_α decreases and D increases monotonically with increasing c. See explanations of Figs. 7–9 below to interpret these results.

D. Distributions of displacements and broken bonds parametrized by disorder

The particles with relatively large D_j should have a higher probability to undergo large displacements ($\gtrsim \sigma_1$) on the time scale of τ_α. Using $S_j=S_j(t_0)$ in Eq. (2.6) at the initial time t_0, we pick up the particles with $S_j<S$ in the mean-square displacement to define

$$M(S)=\sum_{j=1}^{N}\langle\theta(S-S_j)[\Delta \boldsymbol{r}_j(t)]^2\rangle/N, \tag{2.11}$$

where the small and large particles both contribute to the sum. In Fig. 7, we plot the derivative $M'=dM(S)/dS$ for various σ_2/σ_1 and c, which is the distribution of the displacements as a function of S. The area below each curve is equal to the mean-square displacement $\langle[\Delta \boldsymbol{r}(t)]^2\rangle = \Sigma_{j=1}^{N}\langle[\Delta \boldsymbol{r}_j(t)]^2\rangle/N$. Characteristic features are as follows. (i) In the crystalline states, M' mainly arises from the particle motions around defects and is very small. (ii) In the first series, the area is largest for $\sigma_2/\sigma_1=1.25$ due to enhancement of M' around $S\sim 1$. This indicates a high mobility of the particles with $S\sim 1$, giving rise to the behavior of $F_s(t)$ and $\langle[\Delta \boldsymbol{r}(t)]^2\rangle$ in the upper panels of Figs. 5 and 6. (iii) In the first series, M'decreases with increasing σ_2/σ_1 for not large S ($\lesssim 2$), while it becomes insensitive to σ_2/σ_1 for large S.

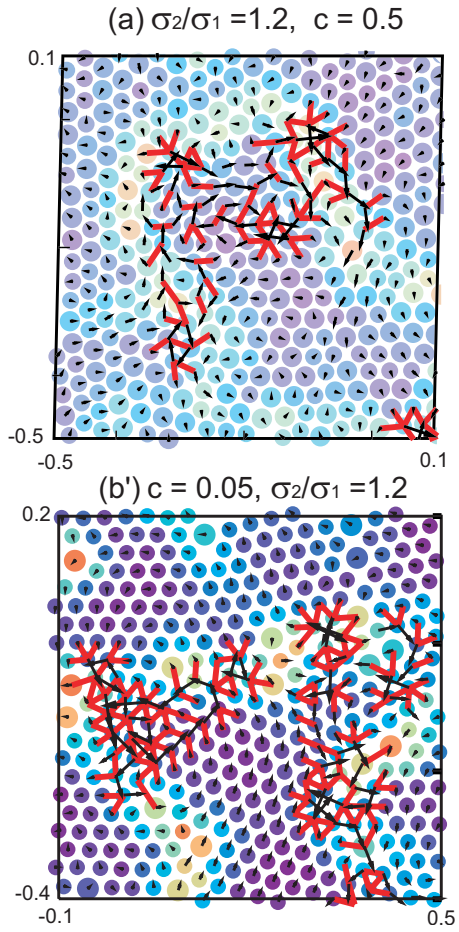

FIG. 8. (Color online) D_j, displacements, and broken bonds in (a) and (b′) of Fig. 2 (the same parts as in Fig. 3). Arrows (in black) denote the displacement for $\Delta t=10^4$, while line segments (in red) are broken bonds. Here most particles in the crystalline region are undergoing small collective motion with their bonds unbroken.

(iii) In the second series, M' increases with increasing c for $S \gtrsim 2.5$, giving rise to the behavior of $F_s(t)$ and $\langle[\Delta \boldsymbol{r}(t)]^2\rangle$ in the lower panels of Figs. 5 and 6.

Another method to visualize the configuration changes at high densities is to introduce "bond breakage" [3]. For each particle configuration given at time t_0, a pair of particles i and j is considered to be bonded if

$$r_{ij}(t_0) = |\boldsymbol{r}_i(t_0) - \boldsymbol{r}_j(t_0)| \le A_1 \sigma_{\alpha\beta}, \tag{2.12}$$

where i and j belong to the species α and β, respectively, $\sigma_{\alpha\beta}=(\sigma_\alpha+\sigma_\beta)/2$, and we set $A_1=1.5$ here. After a time Δt, the bond is treated to be broken if the distance $r_{ij}(t_0+\Delta t)$ exceeds the threshold $A_2\sigma_{\alpha\beta}$ with $A_2=1.75$. In Fig. 8, we display the parts of (a) and (b′) in Fig. 2 (the same parts as in Fig. 3), where the broken bonds written as segments are located around a grain boundary. We recognize that the bonds of the particles undergoing large displacements are mostly broken. However, the bonds between the particles undergoing small collective motion are not broken. In the same manner as in Eq. (2.11) for $M(S)$, we define $B(S)$ such

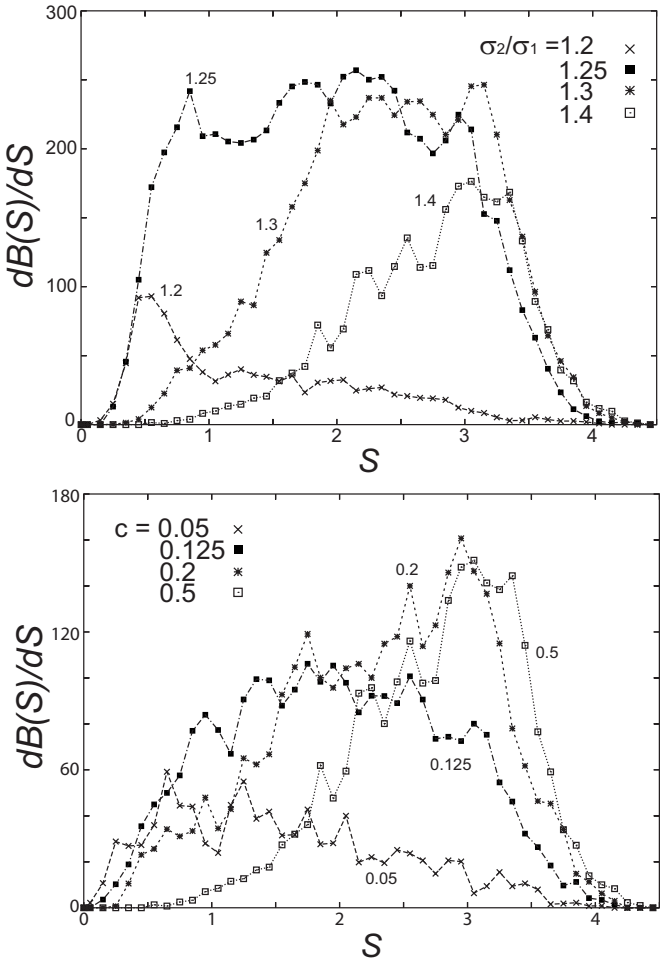

FIG. 9. Distribution of the broken bonds $dB(S)/dS$ as a function of the disorder variable S in Eq. (2.6) for various σ_2/σ_1 (upper plate) and for various c (lower plate). $B(S)$ is defined in Eq. (2.13).

that it is the broken bond number in the range $S_{ij}(t_0) \equiv [S_i(t_0)+S_j(t_0)]/2 < S$. That is,

$$B(S) = \sum_{ij} \langle \theta(S - S_{ij}(t_0))\, \theta(A_1\sigma_{\alpha\beta} - r_{ij}(t_0)) \times \theta(r_{ij}(t_0+\Delta t) - A_2\sigma_{\alpha\beta})\rangle. \tag{2.13}$$

In Fig. 9, we plot the distribution of the broken bonds $B' = dB(S)/dS$ for various σ_2/σ_1 and c with $\Delta t=10^4$. In this quantity, the contribution from the collective motion without bond breakage in the crystalline regions should have been removed, as suggested by Fig. 8. We make comments. (i) It is of interest to compare the curves of $\sigma_2/\sigma_1=1.25$ in Figs. 7 and 9. The peak of M' at $S\sim 1$ in Fig. 7 is much reduced in B' in Fig. 9, but B' there is still not small, suggesting considerable bond breakage at $S\sim 1$ in this polycrystal state. (ii) In the glassy configurations, the contributions around $S\sim 3$ are most dominant. (iii) In the second series, M' in Fig. 7 and B'in Fig. 9 exhibit very similar behavior.

III. SUMMARY AND REMARKS

Using molecular dynamics simulation we have simultaneously visualized the local disorder and the slow dynamics

in polycrystal and glass in a 2D Lenard-Jones binary mixture. We have changed σ_2/σ_1 at $c=1/2$ in the first series and c at $\sigma_2/\sigma_1=1.4$ in the second series, with $T=0.2\epsilon/k_B$ and $\phi=0.9$ held fixed. We summarize our main results and give comments.

(i) Figure 2 demonstrates strong correlations between the disorder variable D_j and the long-time particle displacement. See Refs. [11–13] for similar attempts. The structural heterogeneity represented by D_j is a characteristic feature at high densities and can be seen even in liquid at higher temperatures and even in liquid of one-component systems (see Fig. 10 of Ref. [17]), while the dynamic heterogeneity disappears in liquid.

(ii) For polycrystal-like configurations, the dynamic heterogeneity unambiguously stems from the relatively large mobility of the particles in the grain boundary regions. The dynamics in polycrystal is markedly different in the two series, as in Figs. 5–9. The crystalline regions in the first series are composed of the two components with size dispersity, as in Fig. 3, and are more frustrated than those in the second series.

(iii) In highly frustrated glass, such as for $\sigma_2/\sigma_1=1.4$ and $c=1/2$ in our model, the dynamic heterogeneity emerges on prolonged time scales. The configuration changes in glass are rare thermally activated events and should very sensitively depend on the degree of local disorder which is itself heterogeneous. In (c), (d), and (d′) in Fig. 2, the aggregates of the chainlike motions extend longer than the spatial scale of D_j. We note that no tendency of saturation has been observed in the correlation length of the dynamic heterogeneity with lowering of T in highly frustrated glass [3,7–10]. In our small system, however, we cannot obtain reliable results of the small-q behavior of the structure factor of D_j and that of the broken bonds, while they both decay as q^{-2} at relatively large wave number q [3] (not shown in this paper). In future work, we should thus examine the correlation length of D_j and that of the dynamic heterogeneity at low T in a larger system.

(iv) We may furthermore envisage a crucial role of the local free volume in the slow dynamics. In the literature [22,23], its slow diffusion was supposed to give rise to the aging effects. However, it is difficult to detect such behavior in simulations. In Fig. 3, if the local free volume is identified with the spacing outside the disks, it is nearly randomly distributed in (a) (left) and is mostly around the large particles in (b′) (right). We even notice that a particle densely surrounded by other particles is often pushed out into a new cage. It is worth noting that Widmer-Cooper and Harrowell [12] found no correlation between a local free volume (in their definition using the inherent structure) and the slow dynamics.

(v) We have calculated the functions $n(S)$ in Eq. (2.7), $M(S)$ in Eq. (2.11), and $B(S)$ in Eq. (2.13) and have shown their derivatives dn/dS, dM/S, and dB/dS in Figs. 4, 7, and 9, respectively. These derivatives represent the distributions of the particle number, the displacements, and the broken bonds, respectively, as functions of the parameter S [see Eq. (2.6) for its definition]. The dM/S and dB/dS exhibit similar behavior except the case of $\sigma_2/\sigma_1=1.25$ and $c=1/2$ in the upper panels of Figs. 7 and 9.

(vi) In future work we should investigate the relation between the size ξ and the lifetime ($\sim\tau_\alpha$) of the dynamic heterogeneity for general σ_2/σ_1 and c, which has been done only at fixed σ_2/σ_1 [3,5–11].

(vii) We will shortly report on the rheology of polycrystal states under shear flow. We shall see marked sliding motions of the particles in the grain boundary regions and large collective motions of the small crystalline regions, both being induced by shear.

(viii) In the literature of 2D melting [19,20], the correlation function $g_6(r)$ of the sixfold orientation order has been calculated numerically and experimentally for one-component systems. In our binary systems, its spatial decay becomes shorter with increasing σ_2/σ_1 in the first series and with increasing c in the second series (not shown in this paper). In particular, the algebraic decay $g_6(r)\sim r^{-1/4}$ follows for $\sigma_2/\sigma_1\sim 1.2$ and $c\sim 0.02$ in the two series, respectively. This decay characterizes a transition from a "hexatic" to liquid state in one-component systems. We could discuss vitrification and melting in the same context in 2D binary mixtures [17,24], where defects are proliferated and D_j can be a convenient variable to describe these two transitions.

ACKNOWLEDGMENTS

We would like to thank Hajime Tanaka and Takeshi Kawasaki for showing their work on the relation between the local crystalline order and the dynamic heterogeneity in colloidal glass [24]. The calculations of this work were performed at the Human Genome Center, Institute of Medical Science, University of Tokyo. This work was supported by Grants in Aid for Scientific Research and for the 21st Century COE project (Center for Diversity and Universality in Physics) from the Ministry of Education, Culture, Sports, Science and Technology of Japan.

[1] T. Muranaka and Y. Hiwatari, Phys. Rev. E **51**, R2735 (1995).
[2] M. M. Hurley and P. Harrowell, Phys. Rev. E **52**, 1694 (1995).
[3] R. Yamamoto and A. Onuki, J. Phys. Soc. Jpn. **66**, 2545 (1997); Phys. Rev. E **58**, 3515 (1998).
[4] W. Kob, C. Donati, S. J. Plimpton, P. H. Poole, and S. C. Glotzer, Phys. Rev. Lett. **79**, 2827 (1997); C. Donati, S. C. Glotzer, P. H. Poole, W. Kob, and S. J. Plimpton, Phys. Rev. E **60**, 3107 (1999).
[5] Donna N. Perrera, J. Phys.: Condens. Matter **10**, 10115 (1998).
[6] B. Doliwa and A. Heuer, Phys. Rev. E **61**, 6898 (2000).
[7] R. Yamamoto and A. Onuki, Phys. Rev. Lett. **81**, 4915 (1998); J. Phys. Condens. Matter **12**, 6323 (2000).

[8] N. Lačević, F. W. Starr, T. B. Schroder, and S. C. Glotzer, J. Chem. Phys. **119**, 7372 (2003).
[9] L. Berthier, Phys. Rev. E **69**, 020201(R) (2004); S. Whitelam, L. Berthier, and J. P. Garrahan, Phys. Rev. Lett. **92**, 185705 (2004).
[10] A. C. Pan, J. P. Garrahan, and D. Chandler, Phys. Rev. E **72**, 041106 (2005).
[11] K. Vollmayr-Lee, W. Kob, K. Binder, and A. Zippelius, J. Chem. Phys. **116**, 5158 (2002).
[12] A. Widmer-Cooper and P. Harrowell, Phys. Rev. Lett. **96**, 185701 (2006); J. Non-Cryst. Solids **352**, 5098 (2006).
[13] H. Shintani and H. Tanaka, Nature **2**, 200 (2006).
[14] E. Dickinson and R. Parker, Chem. Phys. Lett. **79**, 578 (1981).
[15] L. Bocqueht, J. P. Hansen, T. Biben, and P. Madden, J. Phys.: Condens. Matter **4**, 2375 (1992).
[16] W. Vermöhlen and N. Ito, Phys. Rev. E **51**, 4325 (1995).
[17] T. Hamanaka and A. Onuki, Phys. Rev. E **74**, 011506 (2006). Here the size ratio σ_2/σ_1 is incorrectly written as σ_1/σ_2 in many places.
[18] S. Nóse, Mol. Phys. **52**, 255 (1983).
[19] B. I. Halperin and D. R. Nelson, Phys. Rev. Lett. **41**, 121 (1978); D. R. Nelson, *Defects and Geometry in Condensed Matter Physics* (Cambridge University Press, Cambridge, England, 2002), p. 68.
[20] K. Zahn, R. Lenke, and G. Maret, Phys. Rev. Lett. **82**, 2721 (1999).
[21] To be precise, $\bar{D}$ depends on the time t after quenching the system [17]. Hence we took its average over t in the period $[t_f - t_d, t_f]$ with $t_f = 2.2 \times 10^4$ and $t_d = 2 \times 10^3$.
[22] L. C. E. Struik, *Physical Aging in Polymers and Other Amorphous Materials* (Elsevier, Amsterdam, 1978).
[23] A. Onuki, A. Furukawa, and A. Minami, Pramana, J. Phys. **64**, 661 (2005).
[24] T. Kawasaki, T. Araki, and H. Tanaka (unpublished).